Jens Fredrik Lunde

Electric field distribution in layered polymeric HVDC insulation

Master's thesis in Energy and the Environment

Supervisor: Frank Mauseth

July 2020

NTNU

**Norwegian University of
Science and Technology**

Jens Fredrik Lunde

Electric field distribution in layered polymeric HVDC insulation

NTNU

Norwegian University of
Science and Technology

Preface

This project is the result of a graduating master thesis performed at NTNU during spring 2020. This particular project is performed at the Department of Electric Power Engineering in cooperation with SINTEF Energy Research (LowEmission Research Centre).

Due to the outbreak of the COVID-19 virus, the project has undergone some revisions throughout the semester as a nation-wide quarantine would not allow work in the laboratory for parts of the semester. Theoretical calculations are therefore used as a supplement to the measurements that were performed.

I would like to thank my supervisor Frank Mauseth and my co-supervisor Øystein Hestad for their guidance and assistance during the project, even though the project did not turn out as planned. I would also like to thank Hans Helmer Sæternes, Jorunn Hølto and Torbjørn Ve at SINTEF for their assistance in the sample making process, with the DSC measurements and with the the laboratory measurements and data analysis, respectively.

Trondheim, July 9, 2020

Jens Fredrik Lunde

Abstract

The HVDC power transfer scheme has become more prevalent in recent times as it is the preferred scheme for long range power transfer. As the cable is stressed based on local fluctuations such as ambient temperature and field enhancements, the need for a greater understanding of the underlying mechanisms affecting the cable becomes more emphasized. Flat, layered samples are used for measurements as they can be used to emulate cable joints/terminations which are considered weak points of a cable.

This project will investigate the space charge accumulation and resulting field enhancement of layered polymeric HVDC insulation. The samples are comprised of two layers of *cross-linked polyethylene* (XLPE) where one layer is cross-linked once while the other is cross-linked twice. This is to create a discontinuity of the conductivity between the layers which should facilitate charge trapping. The measurements are performed using the *Pulsed Electro-Acoustic method* (PEA) with an applied voltage of 10 kV and with temperatures of 20, 40 & 60°C. Finally, the viability of using an equivalent RC circuit as a prediction of the field development has been investigated.

The results show that the greatest charge accumulation occurs at 40°C, while the amount of accumulated charges are quite similar at 20 & 60°C. Heterocharges was observed at the cathode for all samples, while homocharges was present at the anode for all samples. At the dielectric interface charges of negative polarity was observed at all temperatures, but more positive charges was observable with higher temperatures. The heterocharges at the cathode lead to a field reduction in the range of 9.1-47.4% while the homocharges at the anode lead to a field enhancement in the range of 6.7-40.4%.

While the system is quite complex and many mechanisms are influencing the results at the same time, a possible reason for the observed results is that the space charge formation increases slower with increasing temperature than the charge detrapping in the samples, possibly as a result of the increasing mobility of the charge carriers. Other influential mechanisms may be the electrode materials, sample morphology, charge transport in the sample and charge injection.

Representing the samples in terms of an RC circuit was discovered to be viable at low temperatures as fewer mechanisms were present. At higher temperatures more mechanisms were observed and the accuracy of the model decreased. More RC branches could be added in order to rectify this, however at the cost of making the model significantly more complex.

Sammendrag

HVDC overføring har blitt mer og mer vanlig ettersom det er foretrukket over HVAC overføring over lengre distanser. Siden kabelen erfarer ulik påkjenning basert på lokale variasjoner innen blant annet temperatur og felt er det nyttig å utføre dybdeundersøker på hvordan disse mekanismene kan påvirke kablene. Flate, lagdelte prøver brukes under målingene siden de kan etterligne kabelskjøter/termineringer som anses å være et svakt punkt på en kabel.

Det er derfor denne masteroppgaven undersøker hvordan romladningsoppsamling og resulterende feltutvikling påvirker lagdelt polymerisk HVDC isolasjon. Prøvene består av to lag *kryssbudet polyetylen* (PEX) hvor det ene laget er kryssbundet én gang, mens det andre er kryssbudet to ganger. Dette er gjort for å danne en diskontinuitet i konduktiviteten mellom lagene for å framprovosere ladningsoppsamling. Målingene er utført ved å bruke *Pulsed Electro-Acoustic method* (PEA) med en påført spenning på 10 kV over prøven og med temperaturer på 20, 40 & 60°C. Til slutt er muligheten for å bruke en ekvivalent RC model som en prediksjon av feltutviklingen vurdert.

Resultatene viser at den største ladningsoppbyggingen forekommer ved 40°C, mens mengden av oppsamlede ladninger ved 20 & 60°C er ganske like. Heteroladninger er observert ved katoden i alle prøver, mens homoladninger forekommer ved anoden i alle prøver. Ved den interne grenseflaten observeres negative ladninger ved alle temperaturer, men mer positive ladninger observeres ved høyere temperaturer. Heteroladningene ved katoden fører til en feltreduksjon mellom 9.1 og 47.4%, mens homoladningene ved anoden fører til en feltøkning mellom 6.7 og 40.4%.

Selv om systemet er svært komplekst og mange mekanismer påvirker resultatene samtidig er likevel en mulig forklaring på de observerte resultatene at romladningsformasjonen øker saktere ved økende temperatur enn ladningsfrigjøringen. Dette kan komme av økende mobilitet i ladningsbærere ved økende temperatur. Andre påvirkende mekanismer kan være elektrodematerialet, prøvens morfologi, ladningstransport i prøven og ladningsinjeksjon.

Å representere prøvene i form av en RC krets viste seg å være mulig på lavere teperaturer siden færre mekanismer er tilstede. Ved høyere temperaturer kan flere mekanismer observeres og nøyaktigheten til modellen synker. For å forbedre dette kan flere RC grener legges til, men dette fører til at modellen blir betydelig mer kompleks.

Contents

1 Introduction

With an increased focus on long range power transfer comes an increased interest in the HVDC power scheme due to the significant advantages this scheme presents compared to the HVAC scheme. Although HVDC substations are more costly than HVAC substations, advantages such as lower losses at equal conductor current, lower cable cost for equal power transfer due to reduced amount of conductors and the non-necessity for reactive power compensation makes HVDC the preferred scheme for long range power transfer [1] [2, Ch.14].

When DC voltage is continuously applied to a system, an inherent trapping of space charges occur in the insulation. These charges affect the local field of the insulation which could be problematic in case of a short circuit or voltage polarity change. The discharge of the trapped charges depend upon the depth of the trap, meaning the charges can remain in the insulation for long periods of time even if no voltage is applied.

Due to the aforementioned reasons, it is of interest to further investigate the mechanisms of space charge accumulation in HVDC cable systems. In this project, samples of the HVDC material *cross-linked polyethylene* (XLPE) is used. Depending upon the load of the cable as well as the ambient temperature of the surrounding environment, different conditions may apply to different parts of a cable, meaning different rates of space charge accumulation may occur. The effect of temperature on the accumulation of space charges is therefore investigated further in this project.

The samples are layered, where one of the layers is cross-linked once, while the other is cross-linked twice. This is to create an internal interface in the sample to mimic a cable joint, which is considered a weak point of a cable.

This master project has a related preceding specialization project where the effects of applied voltage as well as the internal interface were studied. An increase in the accumulation of space charges was found to correlate with an increase in the applied field, but an insufficient amount of different voltage levels were applied in order to make any trends. Few conclusions were able to be drawn with regards to the internal interface, however theory emphasizes the difference in two materials' conductivity and permittivity as the main factors for space charge build-up at a dielectric interface.

2 Theory

Before the introduction of the experiments and the following analysis of the results, it may be useful to present theory which serves as the basis for the experiments. This chapter will review relevant theory which is used when discussing the acquired results. Note that most of the theory was previously presented in the specialization project preceding this master's thesis, and only minor additions or corrections have been made to the section [3].

2.1 Dielectric properties of a material

A perfect dielectric material may be defined as a material which has no transport of charge carriers, meaning electrons, holes or ions, as well as a permittivity which is independent of frequency and temperature [4]. However, in reality the perfect insulator does not exist which means there will always be some charge carrier transportation through the insulation. Polymer is a popular choice as an insulation medium and will be the focus of this project, so it will be used for further explanation of dielectricity [4].

In the 90s there was a large ongoing operation from cable manufacturers to phase out the common oil-paper insulated cables in favor of extruded cable insulation. This led to the expansion of the polymer-based cable insulation, usually based on polyethylene. The extruded cables had some advantages compared to traditional oil-paper cable insulation, like [1,5]:

- Higher conductor temperatures, giving a more compact cable at the same power rating

- A lighter cable due to lighter moisture barriers

- Easier process when adding joints

- No pollution related to oil-leaks

- Lower cost

When making an extruded cable you may either use pure materials or materials with additives to improve certain properties of the cable insulation. The pure insulation typically suffer from undesirable properties such as high space charge accumulation or a high temperature dependence with regards to its breakdown voltage, leading to an abandonment of this type of insulation in favor of insulation containing proper additives [1].

The additives in polymeric cable insulation may be divided into several categories depending on their function. These categories are [6]:

- *Auxiliaries*, which generally include catalysts used in crosslinking and as emulsifying agents. Some of these may only be used during the manufacturing process and only have remaining residues while others remain in the insulation after the manufacturing process.

- *Additives*, which are added in small concentrations, generally less than 10%, and does not substantially alter the structure of the polymer but changes some of its properties. The additives may include *lubricants* and *parting agents* to improve flow characteristics, *stabilizers* for heat- and ultraviolet-protection, *antioxidants* to prevent oxidation, *flexibilizers* to improve toughness, etc.

- *Compounding ingredients* are added in large concentrations, typically 10-70%. They are divided into two sub-groups: *fillers* and *plasticisers*. Fillers are used to reduce the cost of the insulation while also improving some of its mechanical properties and electrical insulation characteristics. Plasticisers are generally used to reduce the brittleness of the insulation.

Using proper additives may lead to the insulation having outstanding electric properties such as the ones listed in table 2.1:

Table 2.1: Typical electric properties of XLPE cable insulation [4]

	XLPE
Dielectric loss factor, $tan(\delta)$	$1.5 \cdot 10^{-4}$
Insulation resistivity, ρ	10^{19} Ω cm
(Theoretical) Breakdown strength, E_g	500 kV/mm

Comparing this to older mass-impregnated cables which could have an impulse breakdown strength of $110\frac{kV}{mm}$ and a resistivity of $\approx 10^{14}\Omega cm$, the advantageous properties of XLPE cable insulation are highlighted [7].

2.2 Conductivity

The conductivity of any given material may be defined as the transport of charge carriers through a medium, that being either electrons, holes or ions. When applying a DC field, the charge transport is dependent on the conductivity σ and can be expressed by [8]:

$$J = \sigma E \tag{2.1}$$

3

where J is the current density. For a polymer the conduction mechanisms are rather complex because of its semi-crystalline nature [7]. Generally, the conductivity σ varies exponentially with the temperature and can be expressed as:

$$\sigma = \sigma_0 exp(-\frac{\phi}{kT}) = \sum q_i n_i \mu_i \qquad (2.2)$$

where σ_0 is a material constant, ϕ is the activation energy, k is the Boltzmann constant, T is the temperature, q_i, n_i and μ_i is the charge, density and the mobility of the i'th carrier, respectively. This shows how many factors play a part in the determination of the conductivity of the material, meaning it might depend upon the samples preparation and thermal history, making it difficult to determine the conduction mechanism [7].

2.3 Space charges and electrical fields

When applying a voltage over a material, an electric field arises. For homogeneous, flat materials the electric field can be expressed as:

$$E = \frac{U}{d} \qquad (2.3)$$

where U is the applied voltage and d is the width of the material.

With an applied AC voltage, the above expression is sufficient to represent the electrical field, but in DC conditions the applied voltage is constantly of the same polarity and amplitude. Charge carriers in the insulation may then be trapped in the material, creating space charges. Space charges are a discrepancy in the amount of charges going in and out of an area and is an unwanted property. The accumulation of space charges are increased at the electrode-polymer interface as well as internal interfaces of the insulation, meaning the condition of the interfaces are crucial factors. In the bulk of the insulation, space charges may arise due to ionisation of impurities [7]. The space charges increase the local field and if the charge density is sufficiently high, the electrical field may exceed the breakdown strength of the material, leading to failure [1]. The DC electrical field may now be expressed as [9]:

$$\vec{E}_{DC} = \vec{E}_{AC} + \vec{E}_\rho \qquad (2.4)$$

where $\vec{E}_\rho$ is the additional field due to the accumulated space charges. The space charge density ρ can be expressed as [4]:

$$\rho = div\vec{D} \qquad (2.5)$$

4

where $\vec{D}$ is the electrical flux density. It can further be defined as:

$$\vec{D} = \varepsilon_r \varepsilon_0 \vec{E} \tag{2.6}$$

where ε_r is the relative permittivity of the material and ε_0 is the permittivity in vacuum. Combining equation 2.5 and 2.6 gives:

$$\rho = \nabla(\varepsilon_r \varepsilon_0 \vec{E}_\rho) \tag{2.7}$$

Recognizing that

$$\vec{E} = -\nabla \phi_n \tag{2.8}$$

where ϕ_n is the potential at point n, gives Poisson's equation, expressed by:

$$\nabla^2 \phi = -\frac{\rho}{\varepsilon_r \varepsilon_0} \tag{2.9}$$

which might also be useful when calculating the field.

The field enhancement factor $F_{E\%}$ is typically used to describe the local enhancement in the electric field caused by the accumulated space charges. The factor is a percentage value of the increase or decrease in the field, where for flat objects it is represented as [9]:

$$F_{E\%} = \frac{E_{max} - \frac{U_0}{d}}{\frac{U_0}{d}} 100 \tag{2.10}$$

2.3.1 Classification of space charges

The accumulated space charges are usually expressed differently according to the polarity of the space charge in regard to its adjacent electrode. Space charges with equal polarity to that of the adjacent electrode are regarded as homocharges while those with opposite polarity are regarded as heterocharges [7]. A brief description of the two classifications and their significance follows.

2.3.1.1 Homocharges

When the charge has the same polarity as the adjacent electrode it is called a *homocharge*. Effectively, this means that the dielectric is unable to conduct the charges faster than they are injected, leading to the accumulation of equal polarity charges at the electrode [1,10]. This leads to a decreased field at the interfaces, but a higher field in the bulk of the insulation, presented in figure 2.1a.
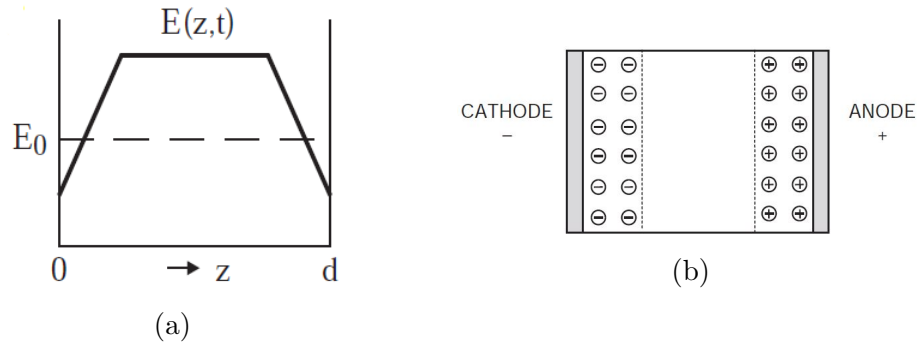
Figure 2.1: *(a)* Electrical field distribution of electrode gap under influence of homocharges where $E_0 = \frac{V_0}{d}$ and *(b)* is a representation of homocharges in terms of the charges at the electrodes [1].

2.3.1.2 Heterocharges

Heterocharges occur when the polarity of the charge is of the opposite polarity of the adjacent electrode. This means that the interfaces are unable to convey the charges at the same rate as the dielectric is able to conduct them. The electrons and positive charges migrate towards the electrode of opposite polarity and is trapped at the interface. This leads to an increase in the electric field at the interfaces of the dielectric [1].
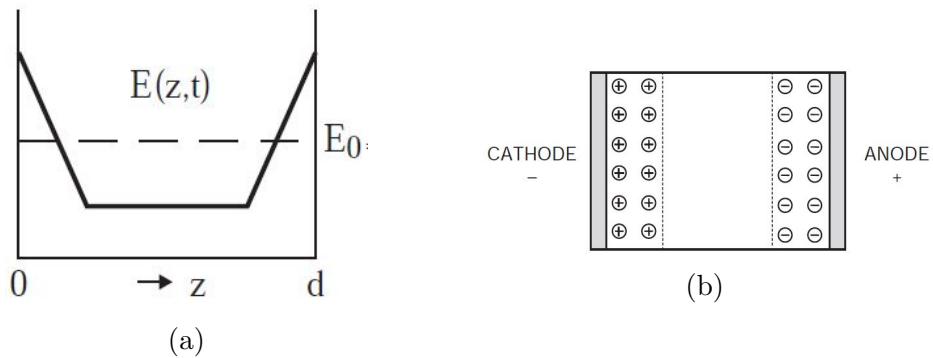

Figure 2.2: *(a)* Electrical field distribution of electrode gap under influence of heterocharges where $E_0 = \frac{V_0}{d}$ and *(b)* is a representation of heterocharges in terms of the charges at the electrodes [1].

2.3.2 Polarisation

Polarisation is a temporary alignment of dipoles in the dielectric caused by an externally applied electrical field which causes a change in the flux density, varying with time. The polarisation may either vanish instantly after

the field is removed, a so-called *momentary polarisation*, or it may gradually decrease with an exponential time constant τ, known as a *relaxation mechanism*. Following are short descriptions of the four different polarisation mechanisms which may be present in a dielectric [4].

Electronic polarisation
When an electric field is applied to a dielectric, the individual atoms are affected. As the electrons are orbiting the nucleus, the negatively charged electrons tends to drift closer to the positive electrode under the effect of the electric field while the positively charged nucleus tends to drift towards the negatively charged electrode. This creates a temporary induced dipole proportional to the electric field. This effect is temporary and is considered a momentary polarisation [4].

Ionic polarisation
Materials comprised of ionic bonded atoms have no inherent dipoles. However, when placed in an electric field, the positively charged ions drifts towards the negative electrode, while the negatively charged ions drifts towards the positive electrode, creating a lattice distortion. This induces a temporary dipole in the material which vanishes when the field is removed. This is therefore considered as a momentary polarisation [4].

Orientational polarisation
Some substances comprised of permanent dipoles such as water have no inherent polarisation under normal circumstances, due to the molecules having a non-symmetrical arrangement. Under the influence of an electric field the dipoles may line up, creating a polarisation. The orientational polarisation[1] can be considered proportional to the electric field, while also inversely proportional to the absolute temperature for gaseous or liquid substances, while in solids the relationships between the polarisation, electric field and temperature are more difficult to determine. After removal of the field, the dipoles will slowly descend back into disorder, meaning this is a relaxation mechanism [4].

Interfacial polarisation
At any section of a dielectric where there is an interface between two differing materials and an electric field is applied, charge build-up may occur due to differing values for the permittivity and conductivity of the two materials. This effect is also known as the Maxwell-Wagner-Sillars effect. The phenomenon may also be caused by additives in the dielectric such as fillers

---

[1]Also known as the dipole- or molecular polarisation

or impurities in the bulk of the material. This mechanism is only relevant for external electric field at sufficiently low frequencies as the movement of charges are not able to follow the changing polarity for higher frequencies. This is considered as a relaxation mechanism [4, 11] [12, Ch.5].

2.4   Charge injection

The concept of charge injection and transport in polymers may be defined in two different ways; ionic- and electronic conduction. For any given material the relevant charge carrier is dependent on several internal- and external factors such as: the materials chemical- and physical composition, frequency of the applied field and temperature, among others [6].

2.4.1   Band theory applied to polymers

A useful way of explaining band theory when considering polymers is to apply Niels Bohrs model of atoms. It states that electrons are only allowed certain discrete energy levels corresponding to different orbitals in the model. The material may either absorb energy, exciting electrons to higher energy levels, or emitting energy leading an electron to "drop" energy levels. The highest filled energy band during absolute zero conditions is called the *valence band*, while the first unoccupied band is called the *conduction band*. Between the two bands is the *band gap*, sometimes known as the *forbidden band gap*[2]. The size of the band gap determines the materials ability to conduct electricity, exemplified by insulators having a band gap greater than 2 eV[3], semi-conductors being in the region of 0.2-2 eV and conductors less than 0.2 eV [6].

Impurities in the polymer gives rise to incompletely-bound atoms which in turn creates so-called *dangling bonds*, which can be satisfied by adding or removing an electron (or both), effectively allowing it to behave as a state in the band gap. Electrons or holes entering the localized states are therefore not available for conduction purposes and may have to acquire considerable amounts of energy to escape these states. They are therefore known as *traps*. The traps may be classified by their trapping "target", either donors for hole traps, acceptors for electron traps or sites where the field from a hole or electron can reorientate the local structure known as a self-trap. The "deeper" the trap, the longer a charge carrier spends in said trap, meaning deeper traps require more energy to free the charge carrier. Self-traps are a

---

[2]Due to the fact that electrons are unable to acquire energy in this region.
[3]Electron volts

form of space charge, meaning it causes a local field enhancement, which can be calculated using Poisson's equation presented in equation 2.9, however with the considerations of equation 2.8 it can be expressed as such [1, 4, 6]:

$$\nabla E = \frac{\rho_c}{\varepsilon} \tag{2.11}$$

where ρ_c is charge density, typically measured in C/m^3 and ε is the permittivity.

2.4.2 Ionic conduction

Ionic conduction entails mass transport of charged atoms through structural defects or interfaces of a material. Ionic conduction can not operate without a steady supply of ions, which means they may either be created by electrolytic actions at the electrode/interface or by decomposition of the insulator/electrode. Ionic conduction may be divided into two sub-categories [6]:

- *intrinsic conduction* which proceeds by dissociation of main-chain or side groups followed by proton or/and electron transfer through hydrogen-bonded networks.

- *extrinsic conduction* where ions not part of the chemical structure of the material is present in the form of an impurity and permeates through the structure.

2.4.3 Electronic conduction

The process of electronic conduction has mostly been covered previously in this chapter, where the transport of electrons or holes through a band structure facilitates conduction. Electrons are trapped by acceptors while holes are trapped by donors, and to leave the trap the charge need to overcome an energy potential barrier with aid from thermal/phonon excitation. A mechanism for this charge transport can be so-called *thermally activated hopping* where a charge gains sufficient energy to "hop" from one trap to the next. Another mechanism is *tunneling*, where the trapped electron can not be defined in a particular location like particles, according to quantum mechanics. In cases where the barrier is sufficiently narrow, the probability of the electron existing on the other side of the barrier is finite, effectively *tunneling* through the barrier [6].

2.4.4 Schottky- and Fowler-Nordheim injection

For injection of charges from an electrode to the polymer to occur, a coulombic potential barrier must be overcome [1]. The charges are thermoionically excited by the applied electric field at the electrode in order to overcome the barrier with height Φ in figure 2.3 [1, 7]. The applied field affects both the height and width of the potential barrier.

Schottky injection is primarily considered in *low field* situations up to 10^9 V/m [6]. It describes how when the height of the potential barrier is reduced, the probability of electrons having sufficient energy to clear the barrier increases [1,7]. The current density J in this instance can be expressed as such [7, 13]:

$$J = AT^2 exp(-\frac{\Phi - \beta_s \sqrt{E}}{kT}) \, , where \, \beta_s = \sqrt{\frac{q^3}{4\pi\varepsilon_0\varepsilon_r}} \qquad (2.12)$$

where A is the Richard-Dushman constant[4], ε_0 is the permittivity of free space, ε_r is the dielectric permittivity and E is the applied electric field.
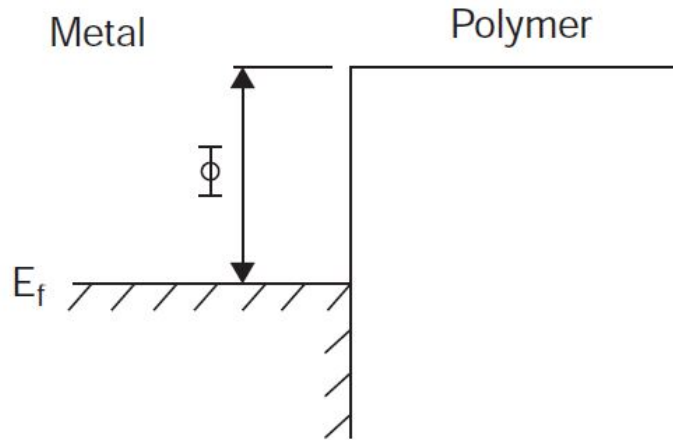

Figure 2.3: Simplified representation of potential barrier at metal-polymer interface [1].

Fowler-Nordheim injection is relevant when the field is sufficiently large ($> 10^9$ V/m) as the theory for the Schottky injection mechanisms breaks down at that point [6]. It states that the width of the potential barrier at

---

[4]$A = 1.2 * 10^6 Am^{-2}K^{-1}$

this point is sufficiently thin as to facilitate electron tunneling through the barrier [1, 6].

2.5 Detection of space charges

For detection of space charges in the test objects, the *Pulsed Electro-Acoustic Method* (PEA) is used. Even though there are other methods for space charge detection, this is the most widely used because it is cheap, simple in structure and easy to implement [14].

The working principle of the PEA method is presented schematically in figure 2.4. After a while under DC conditions, space charges will accumulate in the dielectric. The sample with thickness d is placed between two electrodes and an electrical pulse $V_p(t)$ is applied. The electrical pulse causes slight perturbation from the charges and this perturbation creates an acoustic wave which propagates through the material at the speed of sound towards the detecting electrode. The acoustic signal is detected by a piezo-electric transducer and is transformed into the time-dependant electrical signal $V_s(t)$ [14–16]:

$$V_s(t) = K[\sigma_1 + \sigma_2 + v_{sa}\Delta T \rho(x = v_{sa}t)]e_p \tag{2.13}$$

where σ_1 and σ_2 are the surface charges at the electrode, v_{sa} is the sound velocity through the material, ΔT is the width of the pulse, ρ is the bulk charge and e_p is the amplitude of the pulse voltage.
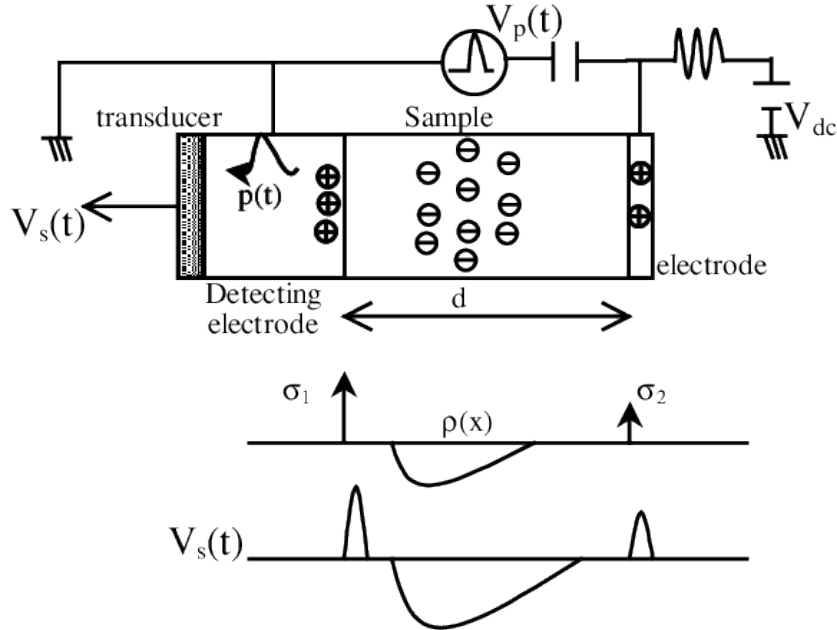

Figure 2.4: Working principle of the PEA method [15]

11

2.5.1 Attenuation and dispersion

Polymeric materials are generally considered as lossy, meaning acoustic waves propagating in the media will be distorted. The waves might experience attenuation and dispersion when propagating through the test object. The attenuation of a propagating acoustic pulse affects the pulse by decaying the amplitude of the pulse through the medium while also introducing a time dependent broadening of the signal [7, 17]. In figure 2.5a, an acoustic pulse with an amplitude of 1 N/m^2 and duration of 30 ns is applied to a non-dispersive medium with an attenuation factor of zero, while in figure 2.5b the same pulse is applied to a medium with a frequency dependent attenuation factor. In the latter case a significantly decaying amplitude can be observed while the pulse is also broadening compared to the former case [17].
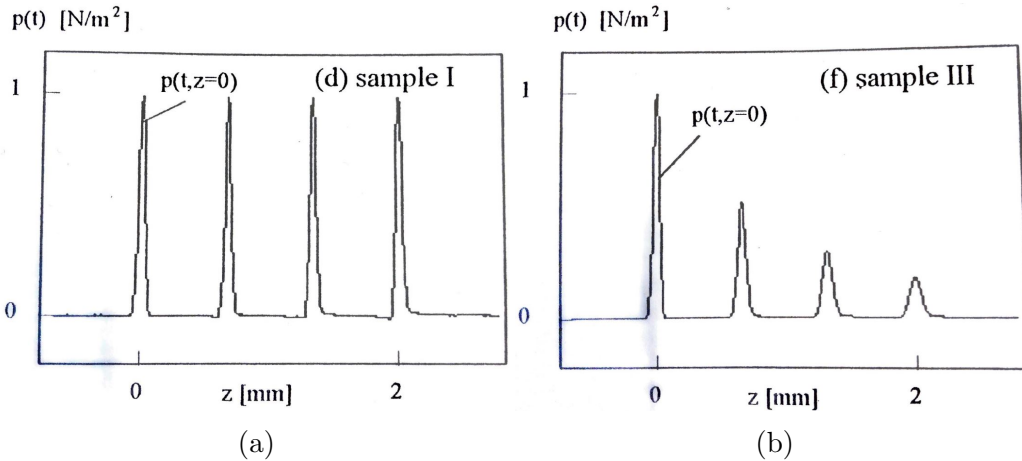

Figure 2.5: *(a)* Acoustic pulse without attenuation in the medium and *(b)* acoustic pulse with attenuation in the medium [17].

For dispersive media, the pulse velocity is a function of the frequency. This might mean that high frequency components of the pulse can be observed in front of- or behind the low frequency components [7, 17]. In figure 2.6a the same pulse as in figure 2.5 is applied to a medium without attenuation. In this case all frequency components propagate with the same velocity. The same pulse is applied in figure 2.6b, however the velocity of the pulse is increasing with frequency. The high-frequency components can therefore be observed in front of the waveform as these components propagate faster than the low-frequency components [17].
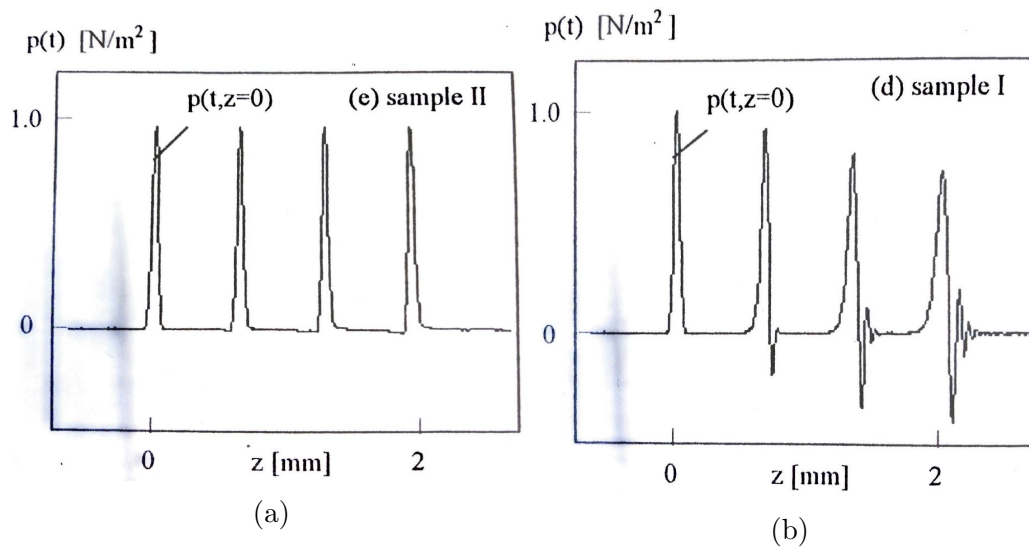
Figure 2.6: *(a)* Acoustic pulse where the velocity of the pulse is not a function of the frequency and *(b)* acoustic pulse where the velocity of the pulse is increasing with frequency [17].

Both attenuation and dispersion will be present in any medium, meaning both factors must be accounted for when analyzing the pulses. In figure 2.7 the same pulse is applied again, but both the attenuation and the dispersion is a function of the frequency. The pulse can now be observed as significantly distorted both in amplitude and duration [17].
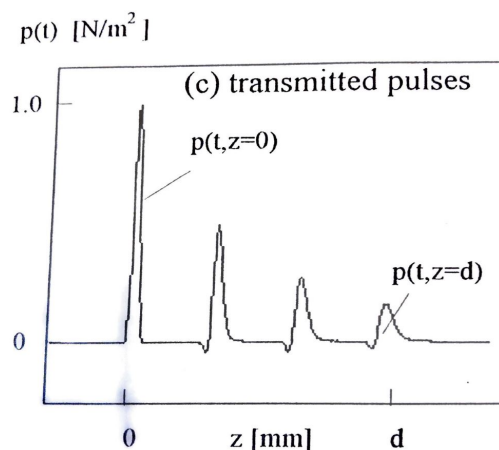

Figure 2.7: Acoustic wave where both attenuation and dispersion is a function of the frequency [17].

13

2.5.2 Calibration

To account for the aforementioned dispersion and attenuation in the material, a calibration of the system is performed. Therefore to achieve quantitative results, the factor K from equation 2.13 has to be determined. In theory, this is quite difficult to accurately calculate due to the complexity of the system. It is therefore usually obtained experimentally [15, 17].

Calibration is performed before each test series by applying a low DC voltage over the sample. Both positive and negative polarity voltages are used to determine the factor K and the surface charges σ_1 and σ_2.

3 Method

This section will present the process of making the test objects as well as the PEANUTS[5] used for space charge measurements. Finally, as supplementary material an RC-equivalent circuit was made as a representation of the sample. The test objects are made up of a .25 mm thin sheet of cross-linked DC material[6] cross-linked with a .25 mm thin sheet of the same DC material.

3.1 Layered test objects

The DC material arrives in the form of pellets, meaning they have to be thermally pressed into sheets before further handling. Approximately 4.5 grams of pellets are placed in a mould consisting of an outer ring, a plate and a shim, as seen in figure 3.1.
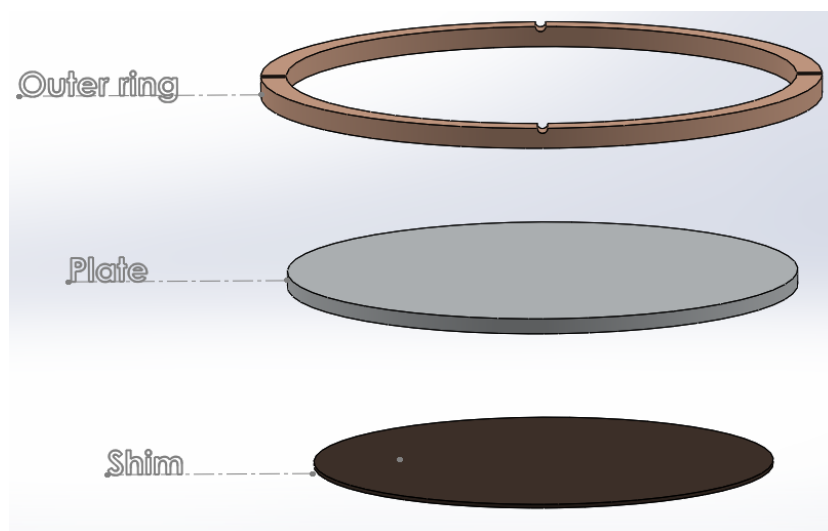

Figure 3.1: Schematic representation of the mould

To cross-link the sample straight from pellets, they are treated in the thermal press using the program presented in table 3.1. A low pressure heating phase is required initially, while the cross-linking occurs at higher pressure and temperature.

---

[5]Pulsed ElectroAcoustic NondestrUctive Test System
[6]LE4253

Table 3.1: Setting of thermal press for cross-linking

-	Pressure [tonnes]	Temperature [°C]	Time [mins]
Low pressure	3.5	120	10
High pressure	25	175	30
Water cooling	25	-	18

A different program is used for the non-cross-linked layer, presented in table 3.2. The pellets are melted at low pressure like in the previous case, however as cross-linking is not the objective, the high temperature and long high pressure phase is not required.

Table 3.2: Setting of thermal press for non-cross-linking

-	Pressure [tonnes]	Temperature [°C]	Time [mins]
Low pressure	3.5	120	10
High pressure	25	120	2
Water cooling	25	-	10

To complete the test objects, the two layers are cross-linked together using the program presented in table 3.3. No low pressure melting is required in this case as the samples are already in the form of sheets.

Table 3.3: Setting of thermal press for layered cross-linking

-	Pressure [tonnes]	Temperature [°C]	Time [mins]
Low pressure	3.5	120	2
High pressure	25	175	30
Water cooling	25	-	18

3.1.1 Degassing

The cross-linking process produces unwanted residues which in turn may facilitate the accumulation of space charges during testing. To combat this issue, both the thin cross-linked samples and the layered samples are placed in a vacuum chamber for approximately three days at 90ºC to remove as many of these impurities as possible.

3.1.2 Sputtering

An ion sputter of the type "Jeol Fine Coat Ion Sputter JFC-1100" is used in order to achieve a well-defined electrode on the test object. The sample is

placed in a mask to hold it in place during the sputtering. Each masking plate has a hole in the middle of different sizes to correspond with the required electrode size. The side of the sample in contact with the upper electrode of the PEANUTS system requires a smaller electrode than the one in contact with the sensor electrode. For this reason, one electrode has a diameter of 7 mm while the other is 20 mm. The mask and the sample is placed in a vacuum chamber where the gold is sputtered. The vacuum is regulated in order to maintain a voltage of 1.2 kV and a current of 5 mA. The process lasts approximately 5 minutes on each side.

3.2 Experimental setup

A representation of the PEANUTS system is presented in figure 3.2, which uses the principles presented in chapter 2.5. The upper electrode is connected to a high voltage pulse generator and a high voltage amplifier, while the lower electrode (sensor electrode) is connected to an amplifier for the raw space charge signal which is further connected to the oscilloscope.

The upper electrode along with the sample is clamped to the sensor electrode and placed in a climate chamber. The chamber is used in order to regulate the temperature. The amplifier along with the oscilloscope and the other high voltage equipment are located outside of the chamber.
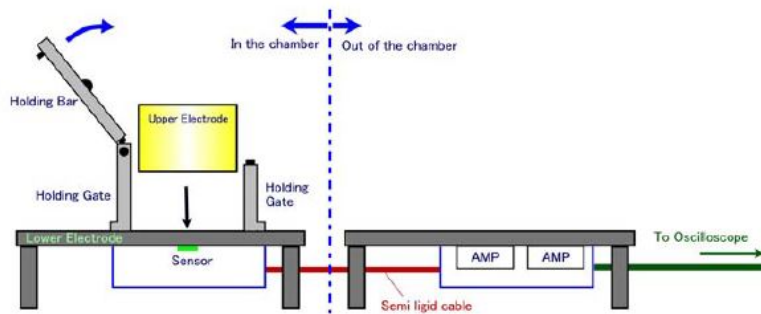

Figure 3.2: Representation of the PEANUTS measurement setup. [18]

A custom program is written in order to execute measurements at the desired intervals. There is a higher concentration of measurements at the beginning of the program, however the number of measurements are reduced after one day has passed. A series typically lasts for one week before the sample is replaced and a new series begins.

The custom program is written to take both *voltage-on-* and *voltage-off* measurements. The *voltage-on* measurements are useful when reviewing the over-

all field distribution, including both momentary- and trapped charges, while the *voltage-off* measurements are useful when reviewing only the trapped charges. In combination they give a complete view of how the charges are trapped throughout the sample and how they affect the overall field while voltage is applied.

To ensure the experimental setup is working properly, a dummy test object is used in combination with a shortened measurement program before any of the proper test series are initiated. By doing this, the execution of the measurement program can be evaluated without waiting for an entire series to finish. In addition, the high voltage- and ground- acoustic matching sheets are replaced on the brass electrode before any test series are initiated to ensure the signal is as good as possible.

3.2.1 Conditioning

Before any new measurement series, the upper brass electrode and the sample are conditioned at the new temperature for approximately one day in order to account for thermal expansion. If the electrode and sample are clamped together before expansion, it might cause an inadequate pressure over the sample which might affect the results. The subjects are therefore placed separately inside the climate chamber. After the conditioning period, the subjects are mounted on the setup and prepared for a second, shorter conditioning period before calibration.

3.2.2 Calibration

As previously stated in chapter 2.5.2, proper calibration of the sample is required for qualitative analysis. A custom program is written in order to record calibration measurements for the samples. Low DC voltages with both positive and negative polarities are applied to the sample for one minute at a time. Voltages of 1, 2 and 3 kV are applied. After calibration, a short discharge period of the sample is executed in order to reduce the charges trapped during calibration.

3.3 RC-equivalent circuit

As the charge accumulation (and as a result, the field distribution) varies significantly throughout the sample, the equivalent circuit is divided into several sections to better represent the different field distortions in a particular region of the sample. Figure 3.3 displays how the sample is divided into the different sections based on the field distortion. A detailed description of

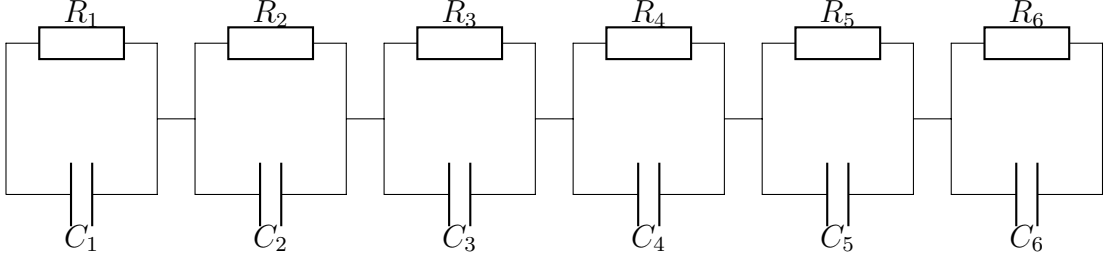the calculated conductivities as well as the values of the RC-components can be found in Appendix A.1.

Figure 3.3: RC-equivalent circuit divided into appropriate sections.

As the sections are divided appropriately as to encapsulate the charge accumulation in the particular region, the sections are of different thicknesses. A detailed description of the different sections and their corresponding equivalent components as well as the thickness of the section is presented in table 3.4.

Table 3.4: Description of the different sections and their corresponding equivalent components.

Section	Equivalent components	Percentage of sample
Cathode	R_1, C_1	10.5
Cathode-bulk	R_2, C_2	26.9
Cathode-interface	R_3, C_3	9
Anode-interface	R_4, C_4	11.1
Anode-bulk	R_5, C_5	29
Anode	R_6, C_6	13.5

The capacitances are calculated using the geometry of the sample. In particular, the equation for parallel plate capacitors is used:

$$C = \varepsilon_r \varepsilon_0 \frac{A}{d} \tag{3.1}$$

where ε_r is the relative permittivity of the sample and ε_0 is the permittivity of free space. The resistance values are approximated under the assumption that the current densities are constant between the sections at steady-state. Equation 2.1 can be modified under this assumption to find the ratio of the conductivities between the sections:

$$\frac{\sigma_1}{\sigma_2} = \frac{E_{DC} + E_2}{E_{DC} + E_1} \tag{3.2}$$

19

where σ_n is the conductivity of a particular section and E_n is the field due to space charges of the same section. The reference conductivity of the single cross-linked layer was previously measured in [19].

4 Results

This section will present both the results of the conducted space charge measurements, as well as the modeling of the resulting field distribution using the RC-equivalent. For the measurements, both the results of the *voltage-on* and *voltage-off* are presented to distinguish between fast and slow charges. Within these categories, both the charge- and field-distributions are presented. A detailed description of the different measurement series are presented in table 4.1. A final series at 80 °C was planned, but due to failing equipment it was not completed. The equivalent RC circuits were designed and simulated using Simulink and compared with the measured results.

Table 4.1: Detailed description of the measurement series.

Test object	L1	L2	L3
Estimated thickness [mm]	0.5	0.5	0.5
Actual thickness [mm]	0.45	0.45	0.45
Applied DC voltage [kV]	10	10	10
Temperature [°C]	20	40	60

4.1 Layered test objects

4.1.1 L1 - 20 kV/mm - 20°C

This section will present the results of the test series carried out on a layered test object at an ambient temperature of 20°C. The applied voltage is 10 kV giving an average field over the sample of 22.2 kV/mm. As of the 5th day of the series, an issue occurred with the scaling of the oscilloscope leading to an inconsistency in the measurements of the charge distribution thereafter. Even though the values of both charges and field at that point are unreliable[7] they are included in the figures anyway as they still show a clear trend for the development of charges.

---

[7]Measures have been taken in order to make these results as cohesive as possible, however the discrepancy is still noticeable, particularly in the *voltage-on* measurements.
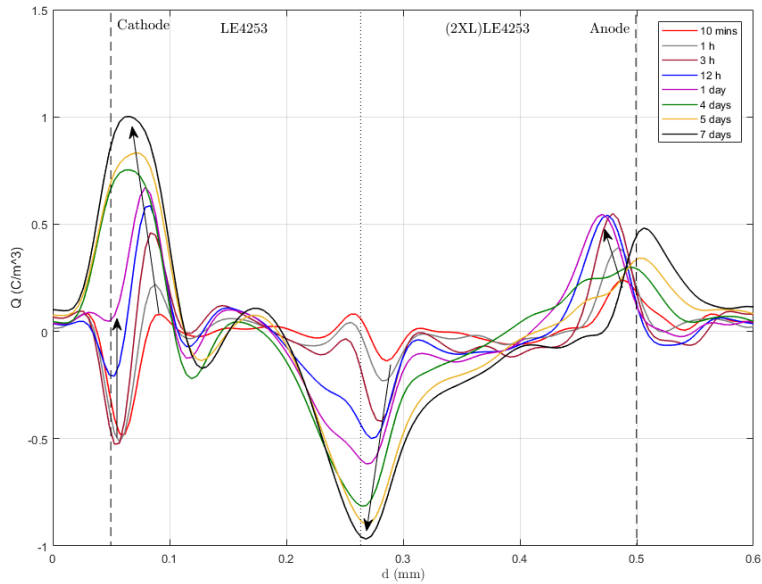
Figure 4.1: Space charge distribution over the layered test object at 20°C for 7 days based on *voltage-off* measurements. Interface between cross-linked and double cross-linked materials is marked with dotted line.

From figure 4.1 there can be observed homocharge build-up at both electrodes after 10 minutes, while at the internal interface minuscule amounts of positive and negative charges build up at the cathode- and anode-side respectively. After approximately 1 day, the net charges at the cathode switches to heterocharges. At the anode the homocharges reaches an apex after approximately 3 hours where it remains relatively stable until 1 day when the net charge accumulation dwindles until 5 days when it starts to increase once again. At the internal interface negative charges builds up quite quickly and continues to increase throughout the series. There is no sign of a slowdown of charge accumulation after 7 days which indicates that a steady-state has not been reached.

Figure 4.2 displays how the slow charges impact the overall charge distribution of the sample. At the cathode the accumulation of heterocharges are signified by the declining apex of the electrode. A leap can be observed between day 4 and 5 signifying the change in oscilloscope setting, however even after the discrepancy, changes can still be observed meaning no steady-state is reached. At the anode the net charge accumulation is quite constant throughout the series, which can be confirmed using figure 4.1 where the development of the charge magnitude at the anode is insignificant compared to the momentary charges. At the interface a gradual build-up of negative

charges can be observed which matches the measurements in figure 4.1.
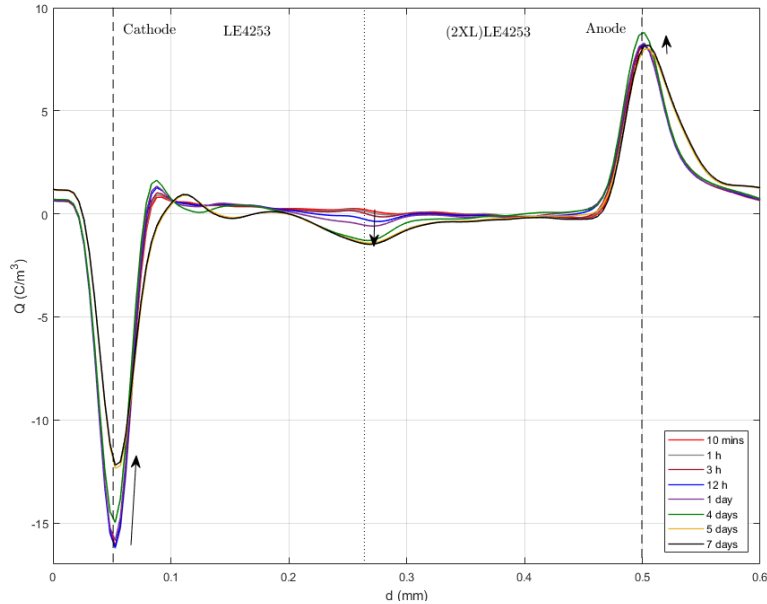

Figure 4.2: Charge distribution over the layered test object at 20°C for 7 days based on *voltage-on* measurements. Interface between cross-linked and double cross-linked materials is marked with dotted line.

Corresponding field

The development of the electric field due to space charges are presented in figure 4.3 while the total field, including both momentary and slow charges are presented in figure 4.4. At the initiation of the series there is a weak negative field enhancement across the entire sample, but as the increase in net heterocharges develops at the cathode the single cross-linked layer experience a field enhancement of opposite polarity as the applied voltage, seen further in figure 4.4. The negative charges at the interface gives a positive field enhancing effect on the double cross-linked layer.

Using equation 2.10 the maximum local field enhancement at the anode is 6.7%, while the local field reduction at the cathode is 9.1%[8].

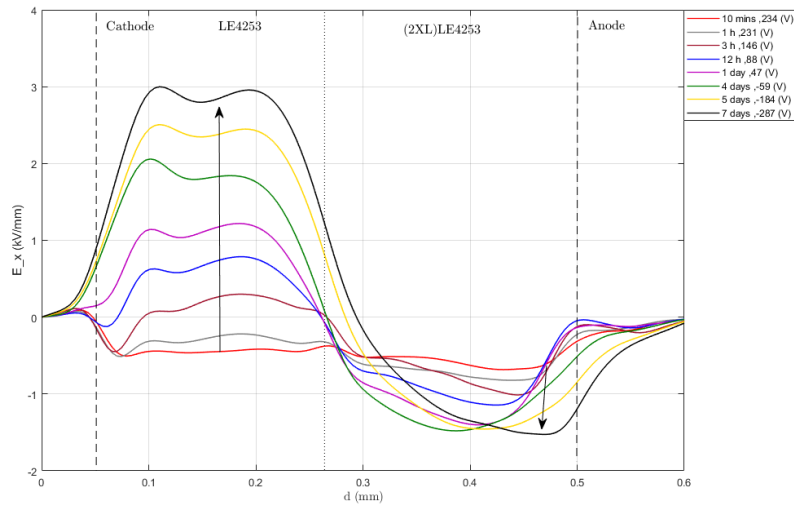[8]Values taken after 4 days due to the aforementioned oscilloscope error.

Figure 4.3: Development of electric field over the layered test object at 20°C for 7 days based on *voltage-off* measurements. Interface between cross-linked and double cross-linked materials is marked with dotted line.
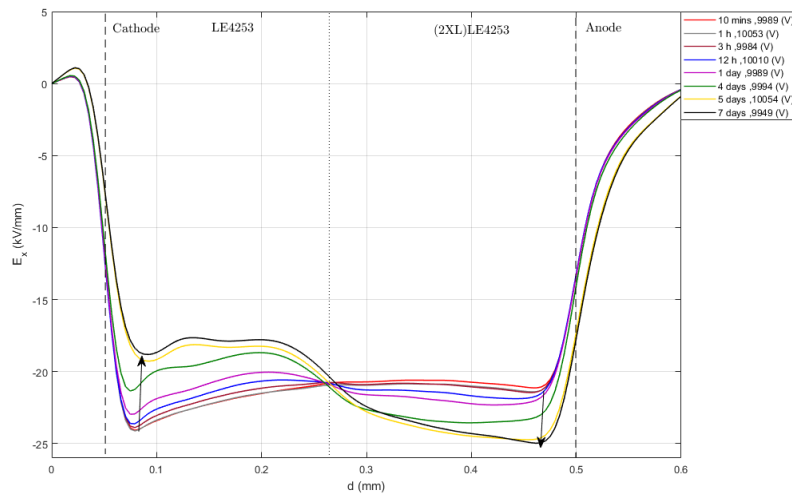

Figure 4.4: Development of electric field over the layered test object at 20°C for 7 days based on *voltage-on* measurements. Interface between cross-linked and double cross-linked materials is marked with dotted line.

4.1.2 L2 - 20 kV/mm - 40°C

This section will present the results of the test series carried out on a layered test object at an ambient temperature of 40°C. The applied voltage is 10 kV giving an average field over the sample of 22.2 kV/mm.
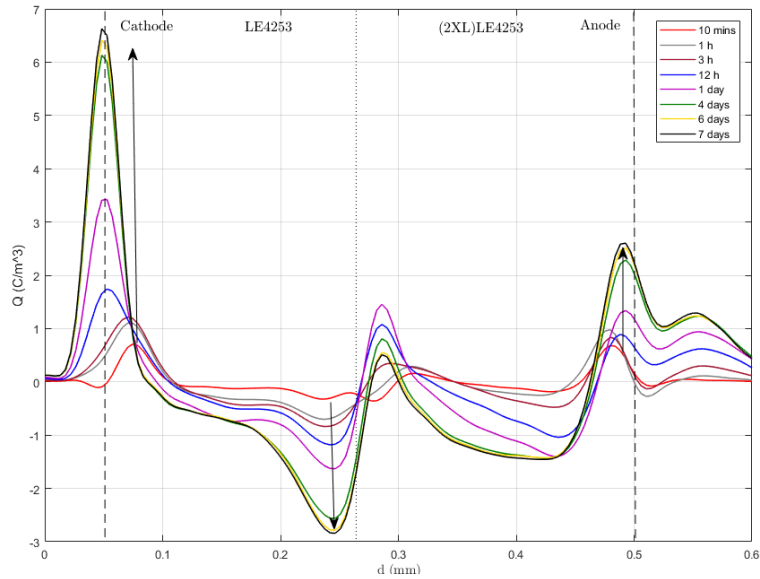

Figure 4.5: Space charge distribution over the layered test object at 40°C for 7 days based on *voltage-off* measurements. Interface between cross-linked and double cross-linked layers is marked with dotted line.

Figure 4.5 shows how a small amount of heterocharges builds up close to the cathode while homocharges of similar amplitude builds up at the anode after a short time. It is worth noting that no significant amount of homocharges can be observed at any point at the cathode. Throughout the series, the heterocharges at the cathode keeps increasing and does not seem to reach steady-state after 7 days, but the accumulation has significantly slowed down at that point. At the anode the homocharges keep increasing in magnitude throughout the series, but not at the same rate as the accumulation at the cathode. At the internal interface, negative charges appear to accumulate at the single cross-linked side with an increasing amplitude throughout the series. At the double cross-linked side, positive charges appear to accumulate, but the amplitude peaks after approximately 1 day, after which it decays for the remainder of the series.

In figure 4.6 the effect of the development of the space charges can be seen on the overall charge distribution. The cathode experience a significant ampli-

tude decay throughout the series, while the anode experience an increase in its amplitude. The negative and positive charges at each side of the interface can also be observed.
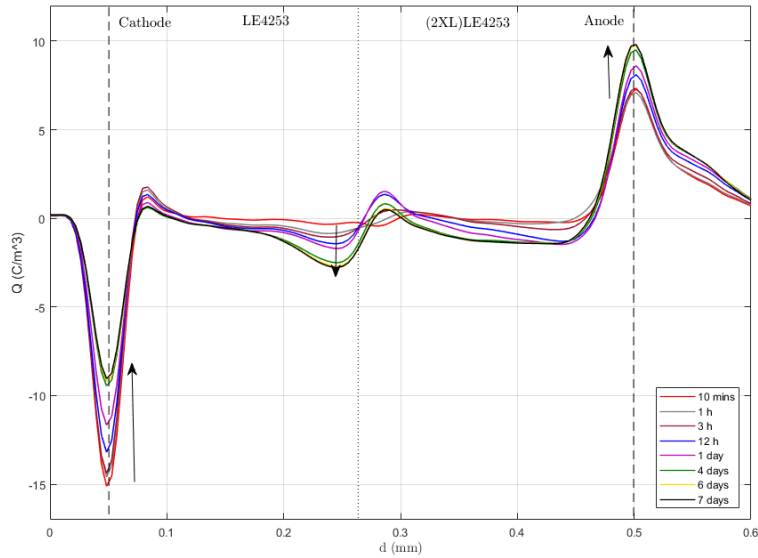

Figure 4.6: Charge distribution over the layered test object at 40°C for 7 days based on *voltage-on* measurements. Interface between cross-linked and double cross-linked materials is marked with dotted line.

Corresponding field

The development of the electric field due to space charges are presented in figure 4.7 while the total field, including both momentary and slow charges are presented in figure 4.8. Throughout the length of the series, the cathode side (single cross-linked layer) experiences a negative field enhancement, continuously increasing in amplitude. Oppositely, the anode side (double cross-linked layer) experiences a positive field enhancement throughout the series. No apparent steady-state is achieved at the end of the 7 days.

Using equation 2.10 the maximum field enhancement at the anode is 40.4%, while the field reduction at the cathode is 47.4%.
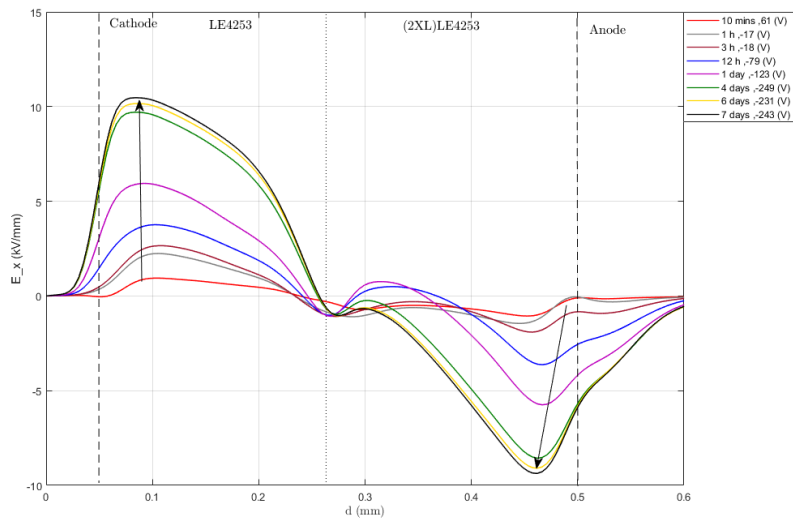
Figure 4.7: Development of electric field over the layered test object at 40°C for 7 days based on *voltage-off* measurements. Interface between cross-linked and double cross-linked materials is marked with dotted line.
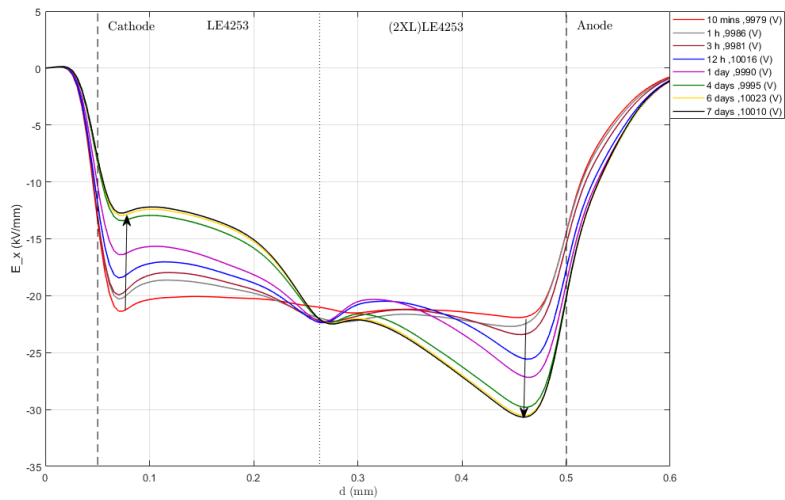

Figure 4.8: Development of electric field over the layered test object at 40°C for 7 days based on *voltage-on* measurements. Interface between cross-linked and double cross-linked materials is marked with dotted line.

4.1.3 L3 - 20 kV/mm - 60°C

This section will present the results from the test series carried out on a layered test object at an ambient temperature of 60°C. The applied voltage is 10 kV giving an average field over the sample of 22.2 kV/mm.
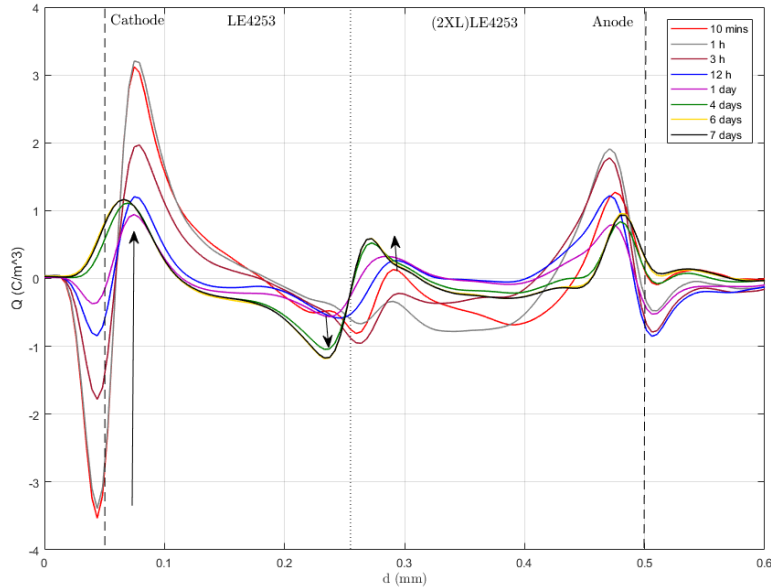

Figure 4.9: Space charge distribution over the layered test object at 60°C for 7 days based on *voltage-off* measurements. Interface between cross-linked and double cross-linked materials is marked with dotted line.

From figure 4.9 it can be observed that a large amount of homocharges build up at the cathode at the beginning of the series. In addition, a similarly large amount of heterocharges build up in the region adjacent to the cathode. Some homocharges can be observed at the anode at the beginning of the series which peaks in amplitude after approximately 1 hour. At the internal interface, some charge build-up can also be recorded at the beginning of the series. Throughout the series the amplitude of the net charges at the cathode decays and after 7 days there is limited development as it reaches a somewhat stable amount of heterocharges. The homocharges at the cathode also decays in amplitude up to 7 days and is relatively stable at this point. Migration of charge peaks in and around the internal interfaces occur throughout the length of the series, but remains relatively stable at the 7 day mark with negative charge build-up at the single cross-linked layer and positive charge build-up at the double cross-linked layer.

The total charge development, including both momentary and slow charges can be viewed in figure 4.10. The peak amplitude at the cathode can be observed after 1 hour, after which it decays throughout the series. The anode experiences a local peak at the initiation of the series and decays in amplitude up to about 12 hours before the amplitude increases until the end of the series. The migration of the charge peaks at the internal interface can be detected, which corresponds with the observations from the *voltage-off* measurements.
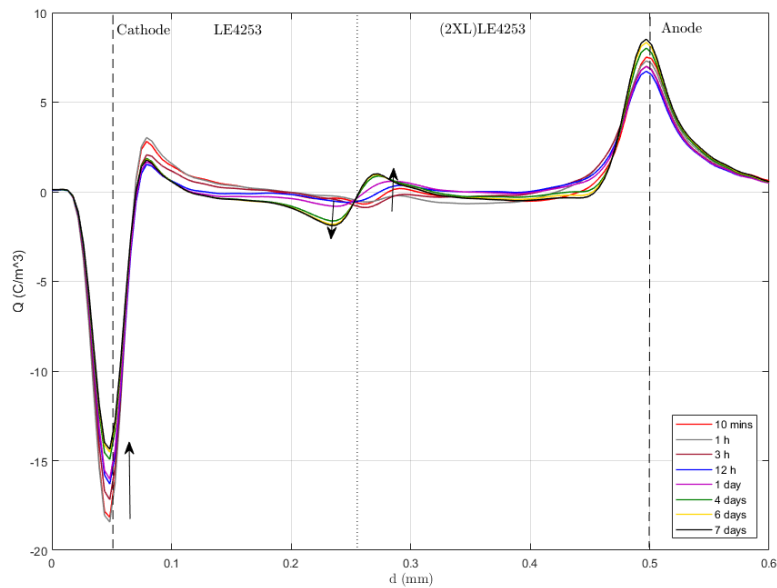

Figure 4.10: Charge distribution over the layered test object at 60°C for 7 days based on *voltage-on* measurements. Interface between cross-linked and double cross-linked layer is marked with dotted line.

Corresponding field

The development of the electric field due to space charges are presented in figure 4.11 while the total field, including both momentary and slow charges are presented in figure 4.12. The accumulation of homocharges at the cathode during the beginning of the series contribute to a local positive field enhancement which turns into a negative field enhancement when the net homocharges develop into net heterocharges. At the anode there is a positive field enhancement after 1 hour, corresponding with the observations from figure 4.9. After this the enhancement decreases until approximately 12 hours before it increases until the end of the series. At the internal interface the field keeps increasing in amplitude throughout the length of the series.

Using equation 2.10 the maximum field enhancement at the anode is 8%, while the local field reduction at the cathode is 16.8%.
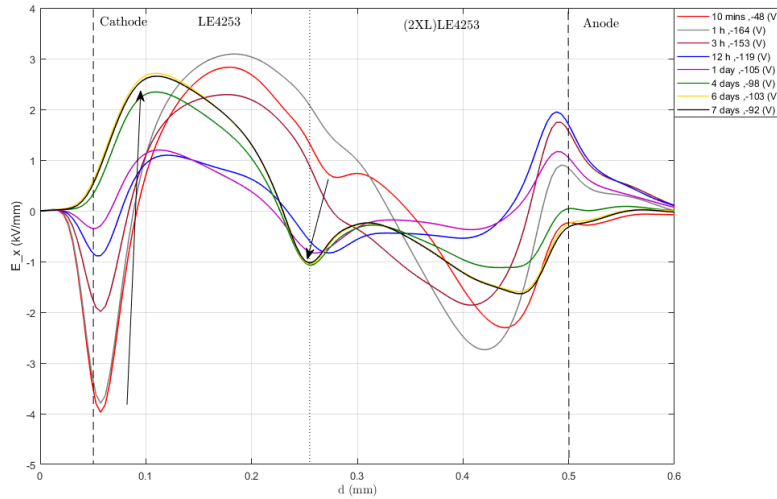
Figure 4.11: Development of electric field over the layered test object at 60°C for 7 days based on *voltage-off* measurements. Interface between cross-linked and double cross-linked materials is marked with dotted line.
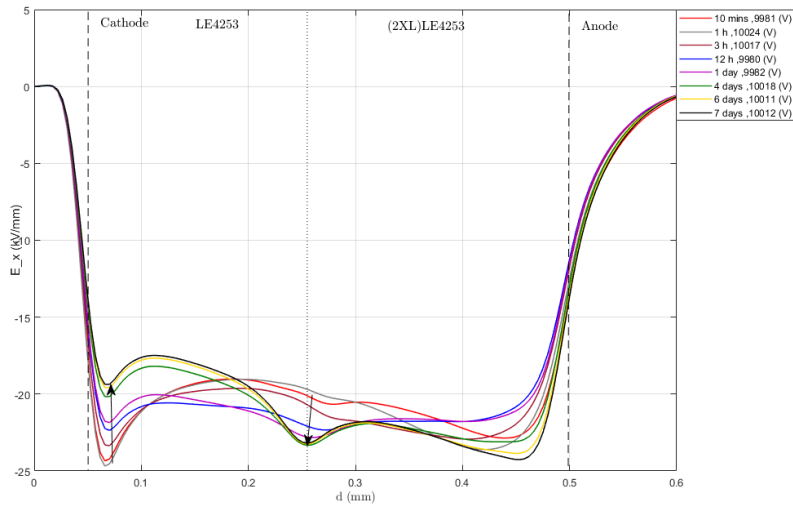
Figure 4.12: Development of electric field over the layered test object at 60°C for 7 days based on *voltage-on* measurements. Interface between cross-linked and double cross-linked materials is marked with dotted line.

4.2 The temperature effect

This section will review the effect the temperature has on the development of the electric field in the samples.
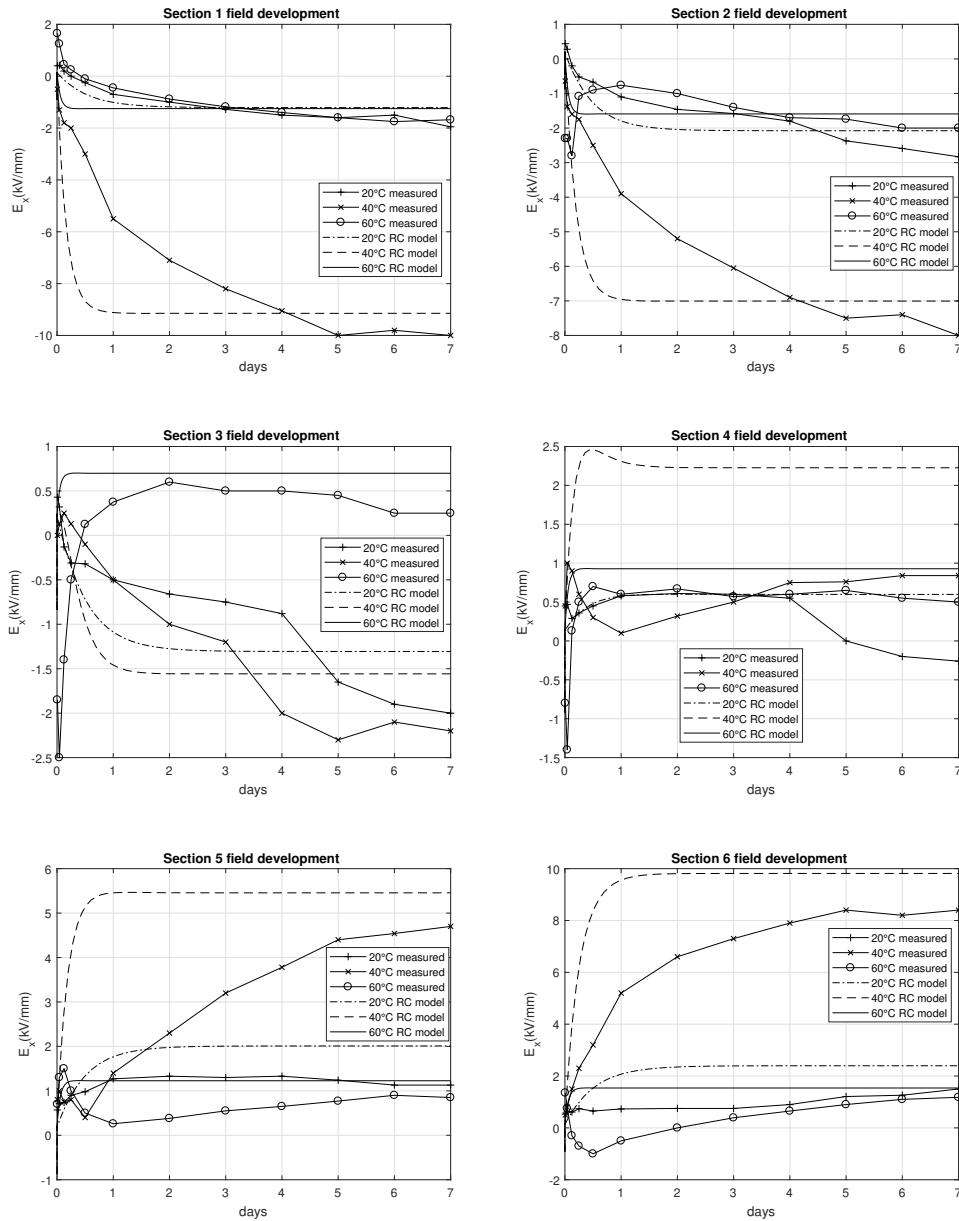
Figure 4.13: Development of electric field due to space charges over time for the different sections of the samples. Results according to the different equivalent RC-circuits are also included.

Figure 4.13 presents the development of the electric field for the different sections of the samples over time. The sections are divided according to table 3.4. It can be observed that the magnitude of the field enhancement is typically greater at 40°C than at other temperatures, while the magnitudes at 20 & 60 °C are approximately the same in value. The exception to this is at the interface sections where all magnitudes are quite similar compared to the other sections. The distribution of all the samples can be related to a Maxwell capacitor, presented by Kreuger in [20]. This generally means that one layer will experience a time-dependent field reduction, while the other will experience a time-dependent field enhancement. While it is not illustrated in figure 4.13, the theory for a Maxwell capacitor also states there will be a time-dependent accumulation of charges at the interface which can be seen in figures 4.1, 4.5 and 4.9.

The development at 20 °C suggests the field follows the charge of a typical capacitor where the charging time is dominated by a time constant τ (demonstrated in [4]). Initially, the field distribution is dominated by the permittivity of the layers, which means there is a capacitive field distribution dictated by the geometry of the sample. Slowly, the field over the sample redistributes into one dominated by the conductivity of the dielectrics, meaning the trend is towards a resistive field distribution. Over time, a quasi steady-state should be reached, however the length of the measurement series does not allow any conclusion to be drawn regarding this matter. It is also worth noting that the same precautions apply for the results of the 20 °C here as previously mentioned, where the results after 4 days are considered unreliable, but are still included to show a general trend.

At 40 °C additional mechanisms can be observed compared to the 20 °C case. At both interface sections as well as the double cross-linked bulk section different accumulation rates can be observed during the first 24 hours of the series. Local peaks generally forms within the first 12 hours before the accumulation reverses for the rest of the series. At the interface of the double cross-linked layer the accumulation also has a second local peak after 24 hours before the accumulation once again reverses.

At 60 °C there are also additional mechanisms compared to the 20 °C case, however not necessarily the same as for the 40 °C case. Particularly at the interface sections a large impulse can be observed up to one hour before the field gradually reaches a quasi steady-state. Similar phenomena can also be observed at the other sections, except for the cathode section, however with a lower peak amplitude.

4.3 RC-equivalent

This section will present the results of the simulations carried out on the RC-equivalent circuit and compare them with the results of the PEANUTS measurements. Results are presented in figure 4.13. As previously stated: the reference conductivity of the single cross-linked layer used for the resistance values is based on measurements performed by Hagen in [19], however it was quite clear that these values would not suffice as the time constant τ of the field development would be way lower than the one observed from the measurements. Previous research on the DC conductivity of XLPE (see ref. [21–24]) suggest large fluctuations in this particular property. Combining these two factors lead to the decision of reducing the calculated value of the different conductivities by a factor of 5 (and in turn increasing the resistance value by a factor of 5) to better fit the curves of the measurements.

The model generally predicts the field development in the different sections correctly, however the magnitude of the enhancement can be slightly off. As the model is highly simplified, it fails to predict the mechanisms occurring early in measurements at higher temperatures. As the field development at 20 ℃ does not show signs of complicated mechanisms, the model fits well with this series.

As the measured time constant appears to vary slightly throughout the sample, the model typically fails to predict the development rate of the field. In some cases, like at the cathode and anode-interface at 20 ℃, the model fits quite well with the measurements, while in other cases, like the anode-interface and anode-bulk at 40 ℃, the model would need significant adjustments to fit the measurements.

5 Discussion

The accumulation of space charges in layered polymeric DC insulation has been investigated alongside the effect temperature has on this phenomenon. All samples are constructed using a layer of XLPE which in turn is cross-linked with a layer of non-cross-linked polyethylene. The PEA method is used to conduct the measurements. Finally, the viability of using an equivalent RC circuit to simulate the field development has been evaluated. This section will investigate the mechanisms for the acquired results.

5.1 Charge development

Electrode-polymer interface

Regarding the electrode-polymer interfaces, slightly different observations can be made for the different temperatures. At 20°C (fig. 4.1) homocharges can be observed at both electrodes early in the series. Over time the net charges at the cathode develops into heterocharges, and after 1 day no homocharges can be observed. The homocharges observed at the anode remain throughout the series, however fluctuating in amplitude. At 40°C (fig. 4.5) homocharges are observed at the anode, however the net charges at the cathode indicate a presence of heterocharges throughout the entire series. At 60°C (fig. 4.9) a significant amount of homocharges are observed early in the series at the cathode with mirrored charges in the adjacent region. Similarly, homocharges can be observed at the anode, although with a lower amplitude, and mirrored charges can be observed at the adjacent region. Within one day, the homocharges at the cathode as well as the mirrored charges amalgamates into net heterocharges with a lower amplitude than what both regions initially had. The same phenomenon can also be observed at the anode where the homocharges and its mirrored charges form net homocharges over time.

As per theory presented previously in this thesis (see chapter 2.3.1) the development of homocharges at the electrode means charge injection occur faster than the dielectric is capable of transporting the charges, while the heterocharge development means the transport occur faster than the injection. The charge injection has been reported to be temperature dependent [25]. The charge injection is also dependent upon several other factors such as the electrode material, dielectric material and residual by-products in the dielectric where any of these factors may also be temperature dependent or vary from sample to sample [9, 26, 27]. Combining all these factors make the charge injection difficult to quantify and attributing the space charge formation to the varying charge injection may be difficult.

However, what can be seen from the measured results is that typically the injection of positive charges at the anode is greater than the transport regardless of the temperature. On the contrary, the transport of positive charges to the cathode will eventually be greater than the injection of negative ones for all temperatures. The reason for the charge polarity switch at the cathode over time has previously been presented by Hagen [19] and may be attributed to electronic transport occurring faster than ionic transport, leading to electronic transport being dominant early in the series while ionic transport slowly becoming more dominant as time passes. Another theory is that different charges have different mobility in the different layers. The theory has previously been presented by Rogti & Ferhat [26] and might mean that positive injected charges at the anode move slower towards the cathode than the negative injected charges at the cathode move in the opposite direction. The dielectric interface may also affect this, but this will be discussed later. The heterocharge scheme which arises is unlikely to be due to the ionization of cross-linking by-products as the samples have been thoroughly treated after cross-linking, meaning the heterocharges are more likely to be attributed to blocking capabilities of the electrode-insulation interface [9]. What remains uncertain is why no homocharge at the cathode at 40°C can be observed at any point.

Dielectric interface
In all series, charges of opposite polarity as the applied voltage accumulate at the dielectric interface. At 40°C negative charges accumulate at the cathode side of the interface with positive charges accumulating at the anode side of the interface, although with a much lower amplitude compared to the negative charges. At 60°C negative and positive charges accumulate at the cathode- and anode-side, respectively, but this time with quite similar amplitudes. The greatest accumulation occurs at 40°C, while the amount of charges are quite similar at 20 and 60°C, so the accumulation does not necessarily increase with increasing temperature.

The theory of Maxwell-Wagner (MW) polarization (see chapter 2.3.2) states that a discontinuity in the conductivity or permittivity of layered specimen may facilitate charge build-up at the interface. Another reason for the interfacial charge build-up has been attributed to the electrode material [26]. If the interfacial charges are mainly due to MW polarization one would expect the two materials to be most dissimilar at 40°C as this is where the most charge build-up occurs. Further investigation into this matter would be of interest going forward.

At lower temperatures negative charges are the main cause for charge accu-

mulation at the dielectric interface. The trend shifts with increasing temperature, as positive charges can be observed at the anode side of the interface and at 60°C the amplitude of the charges at each side of the interface are quite similar. The effect the interface has on charge accumulation has previously been studied by Chen et al. [28] and the interface has been found to be more prone to blocking negative charges than positive ones. When the temperature is increased, an increasing amount of positive charges are blocked at the interface, while more negative charges are blocked at 40°C than 20°C, but drops off drastically when the temperature is increased further to 60°C. It may indicate that negative charges are more capable of transport between the layers at higher temperatures. On the contrary, the transport of positive charges appear to decrease between the layers with increasing temperature. As the PEA system measures net charges, the apparent increase in trapped positive charges at higher temperatures may rather be attributed to a depletion of negative charges at the interface.

Overall charge development
As previously presented, the greatest charge accumulation occurs at 40°C, while the accumulation at 20 & 60°C are quite similar. These results confirm that several mechanisms are contributing to the overall charge development. From research by Bodega [9] the charge accumulation is expected to keep increasing in the temperature range of 20-60°C, which it does not. A possible explanation of this comes from Lan et al. [25] as their research indicated that the space charge formation rate increases slower than the charge detrapping rate as a function of the temperature. What this would entail is an increase in the accumulated charges with increasing temperature up to a certain point where the accumulation would begin decreasing. The mobility of charge carriers has also been observed to increase significantly with increasing temperature, possibly affecting the charge trapping and detrapping rate as well as the conduction. This theory fits well with what has been observed in this project.

The morphology may also affect the acquired results. *Differential Scanning Calorimetry* (DSC) measurements were performed on one of the layered samples and compared with a sample of XLPE, which are presented in appendix A.2 alongside a short explanation of the procedure. The XLPE sample had a degree of crystallinity of 27.9%, while the first layered sample had 33.4% and the second had 31.8%, meaning the double cross-linking process increased the degree of crystallinity. Increasing the degree of crystallinity will in turn reduce the amorphous regions of the sample. Amorphous regions, as well as the interfacial regions between amorphous and crystalline regions have

been reported to be preferred trapping locations for space charges in PE and an important factor when reviewing conductivity of semi-crystalline polymers [1, 29, 30]. The measured charge accumulations in this project (fig. 4.1, 4.5 and 4.9) does indicate a lower amount of charges in the double cross-linked layer compared with the single cross-linked layer. An increased degree of crystallinity could be the causation of this, although further investigation into the matter would be useful before drawing any conclusions. Natural variations in the morphology of the samples may also cause different charge build-up during measurements, meaning additional measurements at the same temperatures would be useful in order to verify the reproducibility of the results during this project.

5.2   Field development

As a result of the accumulated charges, the field in the two layers are distorted. As one might expect from the reviewed charge accumulation, the greatest distortion can be observed at 40°C. The single cross-linked layer experiences an overall field reduction, while the double cross-linked layer experiences an overall field enhancement. Table 5.1 gives a summary of how the field is distorted at the two electrodes at the measured temperatures.

Table 5.1: Summary of the maximum field enhancement and reduction in the test objects at various temperatures. Note that the values at 20°C are from 4 days and not the end of the series.

Temperature	20°C	40°C	60°C
Maximum field enhancement	6.7%*	40.4%	8%
Maximum field reduction	9.1%*	47.4%	16.8%

5.3   RC-equivalent

As previously presented, the model does well when predicting the field development at low temperatures, but loses accuracy when more mechanisms are more prevalent at higher temperatures. Additional RC branches in parallel of each section would be able to more closely represent the different mechanisms, however with each new branch the values in the model would become more complicated to calculate.

As the values of the model are based on results of the measurements, the final value of the measured field has great influence over the calculated resistances. It is assumed in this project that the field development has reached

steady-state at the end of the measurements, however particularly at lower temperatures this assumption may be inaccurate. A longer series may therefore have been more adequate when calculating the RC components to ensure more accurate values.

As the conductivity of the double cross-linked layer has not been measured previously, only estimations can be made of its value. The model could be improved using a more accurate value of the conductivity based on measurements. The accuracy of the previous measurements on the single cross-linked layer can also be called into question. The previous measurements were performed on extruded material, while the material in this project came from pellets. Even though the significance of this detail is questionable, results show clear discrepancies between expected and measured results, enough to warrant a mention. Natural variations in the material itself may also have an effect on the conductivity.

6 Conclusion

The charge accumulation of layered polymeric samples under varying temperatures has been investigated. Charges of opposite polarity as the applied voltage (negative charges) are observed at the dielectric interface in all samples regardless of ambient temperature, but more positive charges are observed at the interface with increasing temperature. The accumulation at the dielectric interface has been observed to be affected by the temperature where the greatest accumulation of negative charges occurred at 40°C. This may be due to the space charge formation rate increasing slower than the charge detrapping rate with increasing temperature. Other mechanisms such as charge injection, transportation, electrode materials and sample morphology have also been discussed as reasons for the varying space charge accumulation with increasing temperature. The complexity of the system is therefore restated and attributing the overall charge development to a particular mechanism would be misleading.

As a result of the accumulated heterocharges at the cathode, a field reduction in this region occurs for all samples. At the anode, homocharges are observed regardless of temperature, always creating a field enhancing effect in this region. The length of each series was too short to verify if the accumulation had reached steady-state at the end of the series.

Simulations of a series of parallel RC components has been carried out in order to investigate the validity of using such a model for a layered polymeric sample. At low temperatures the model fits relatively well with the measured results, however at higher temperatures more mechanisms are prevalent in the measurements making the model less accurate. Additional RC branches can be included in the model to increase the accuracy at higher temperatures, but in doing so will increase the complexity of the model significantly. The accuracy of the model is affected by the duration of the measurement series due to some components being calculated based on the steady-state value of the field in the samples. The accuracy of the model may therefore have been reduced as it is uncertain if the field in the sample had reached steady-state at the end of the series.

7 Further work

It would be of interest to measure the conductivity of the double cross-linked polyethylene material and possibly the layered materials like the ones in this project as well. This may increase the understanding of how charges accumulate based on the conductivity of the layers. It may also be of interest to vary the applied field in addition to the temperature when performing measurements to expand the knowledge of how both mechanisms operate in tandem. Another option is to apply a temperature gradient over the sample to see how this condition affects the space charge accumulation.

Using a semiconducting material as the electrodes may also be of interest moving forward. Semiconducting materials have been reported to have different injection rates than gold or aluminium electrodes and would be a more accurate scenario for cables compared to gold or aluminium.

References

[1] Giovanni Mazzanti and Massimo Marzinotto. *Extruded Cables for High-Voltage Direct-Current Transmission.* John Wiley & Sons, 2013.

[2] Thomas Ackermann. *Wind Power in Power Systems.* John Wiley & Sons, 2nd edition, 2012.

[3] Jens Fredrik Lunde. Electric field distribution in layered polymeric hvdc insulation. Project report in TET4510, Department of Electric Power Engineering, NTNU – Norwegian University of Science and Technology, Dec. 2019.

[4] Erling Ildstad. *TET4160 Insulating Materials for High Voltage Applications.* NTNU Department of Electrical Engineering, 2016.

[5] T.L. Hanley, R.P. Burford, R.J. Fleming, and K.W. Barber. A general review of polymeric insulation for use in hvdc cables. *IEEE Electrical Insulation Magazine*, 19(1):13–24, 2003.

[6] L.A. Dissado and J.C. Fothergill. *Electrical Degradation and Breakdown in Polymers.* The Institution of Engineering and Technology, 2nd edition, 1992.

[7] Bjørn Sanden. *XLPE cable insulation subjected to HVDC stress.* PhD thesis, NTNU, 1996.

[8] T. A. Ve, F. Mauseth, and E. Ildstad. Space charge accumulation in xlpe insulation at high temperature and water content. In *2013 IEEE International Conference on Solid Dielectrics (ICSD)*, pages 435–439, 2013.

[9] Riccardo Bodega. *Space Charge Accumulation in Polymeric High Voltage DC Cable Systems.* PhD thesis, Delft University, 2006.

[10] Frank Mauseth. Dielectric losses and polarisation (2). PPT presentation, NTNU, 2019.

[11] M. Kuriakose, S. Longuemart, M. Depriester, S. Delenclos, and A. Sahraoui. Maxwell-wagner-sillars effects on the thermal-transport properties of polymer-dispersed liquid crystals. *Physical Review E*, 89:022511, 02 2014.

[12] D. Langhe and M. Ponting. *Manufacturing and Novel Applications of Multilayer Polymer Films.* William Andrew, 2016.

[13] H. J. Wintlet. Schottky injection currents in insulators: The effect of space charge on the time dependence. *IEEE Transactions on Electrical Insulation*, EI-12(6):424–428, Dec 1977.

[14] H. Hussaini, A.A. Ahmad, and S.A. Abimbola. Review of space-charge measurement using pulsed electro-acoustic method: Advantages and limitations. *Int. Journal of Engineering Research and Applications*, 5(4):90–95, 2015.

[15] G. Chen, Y.L. Chong, and M. Fu. Calibration of the pulsed electroacoustic technique in the presence of trapped charge. *Measurement Science and Technology*, 17(7), 2006.

[16] Y. Li, M. Yasuda, and T. Takada. Pulsed electroacoustic method for measurement of charge accumulation in solid dielectrics. *IEEE Transactions on Dielectrics and Electrical Insulation*, 1(2):188–195, 1994.

[17] Y. Li. *Space Charge Measurement in Lossy Solid Dielectric Materials By Pulsed Electroacoustic Method*. Musashi Institute of Technology, 1994.

[18] FiveLab. *PEANUTS combined manual*.

[19] Jens Eirik Hagen. *Romladningsdistribusjon i lagdelt XLPE HVDC kabelisolasjon*. Master's thesis, NTNU, 2014.

[20] F.H. Kreuger. *Industrial High DC Voltage*. Delft University Press, 1995.

[21] R. Bodega, G. C. Montanari, and P. H. F. Morshuis. Conduction current measurements on xlpe and epr insulation. In *The 17th Annual Meeting of the IEEE Lasers and Electro-Optics Society, 2004. LEOS 2004.*, pages 101–105, 2004.

[22] Zhiyu Yan, Baozhong Han, H. Zhao, J. Yang, and Chunyang Li. Space charge and conductivity characteristics of cb/xlpe nanocomposites. In *Proceedings of 2014 International Symposium on Electrical Insulating Materials*, pages 30–33, 2014.

[23] S. Trætteberg, E. Ildstad, and R. Hegerberg. *Influence of DC voltage and temperature gradient on the distribution of space charge in XLPE*. Norwegian University of Science and Technology.

[24] Torbjørn Ve, Frank Mauseth, and E. Ildstad. Effect of water content on the conductivity of xlpe insulation. pages 649–653, 10 2012.

[25] L. Lan, J. Wu, Y. Yin, X. Li, and Z. Li. Effect of temperature on space charge trapping and conduction in cross-linked polyethylene. *IEEE Transactions on Dielectrics and Electrical Insulation*, 21(4):1784–1791, 2014.

[26] F.Rogti and Marhoun Ferhat. Maxwell-wagner polarization and interfacial charge at the multilayers of thermoplastic polymers. *Journal of Electrostatics*, 72:91–97, 01 2014.

[27] T. Mizutani. Space charge measurement techniques and space charge in polyethylene. *IEEE Transactions on Dielectrics and Electrical Insulation*, 1(5):923–933, 1994.

[28] George Chen, T. Takada, and Lisheng Zhong. Effect of polyethylene interface on space charge formation. *Dielectrics and Electrical Insulation, IEEE Transactions on*, 11:113 – 121, 03 2004.

[29] Gilbert Teyssedre and Christian Laurent. Charge transport modeling in insulating polymers: From molecular to macroscopic scale. *Dielectrics and Electrical Insulation, IEEE Transactions on*, 12:857 – 875, 11 2005.

[30] Ø. L. Hestad, F. Mauseth, and R. H. Kyte. Electrical conductivity of medium voltage xlpe insulated cables. In *2012 IEEE International Symposium on Electrical Insulation*, pages 376–380, 2012.

A Appendix

A.1 Conductivities and RC-components

Table A.1: Conductivity of the single cross-linked PE layer at relevant temperatures based on measurements from [19].

Temperature	σ [S/m]
20°C	$2.63e - 15$
40°C	$7.55e - 15$
60°C	$2.22e - 14$

Table A.2: Values of the different RC-components used for simulations. Note that these values are the calculated ones and are not adjusted according to the measured results.

Component	20°C	40°C	60°C
C_1		21.7pF	
C_2		8.48pF	
C_3		25.4pF	
C_4		20.4pF	
C_5		7.83pF	
C_6		17pF	
R_1	$373T\Omega$	$107T\Omega$	$43T\Omega$
R_2	$913T\Omega$	$318T\Omega$	$108T\Omega$
R_3	$316T\Omega$	$144T\Omega$	$40T\Omega$
R_4	$431T\Omega$	$213T\Omega$	$50.5T\Omega$
R_5	$1.19P\Omega$	$627T\Omega$	$133T\Omega$
R_6	$558T\Omega$	$335T\Omega$	$62.2T\Omega$

A.2 DSC measurements

The DSC measurements are performed by gradually heating the sample up to its melting point which reveals the thermal history of the sample. As the cross-linking process is exothermic, it can be observed as a negative peak on the DSC curve. The degree of crystallinity of the sample can be calculated from the curves. The uppermost curve in figures A.1, A.2 and A.3 is the first heating of the sample which is performed to remove the thermal history. No substantial changes in the sample occur until the sample is at 90°C which is the temperature the sample is treated at after cross-linking. The second curve gives a better picture of the melting curve without any treatment of the sample. Two measurements on layered samples[9] were performed as the first had a somewhat unexpected melting curve. Comparing the layered samples with the XLPE sample, the onset from the layered samples can be linked with the peak of the XLPE sample as they occur at the same temperature. The second cross-linking process creates the deep peak before the onset.
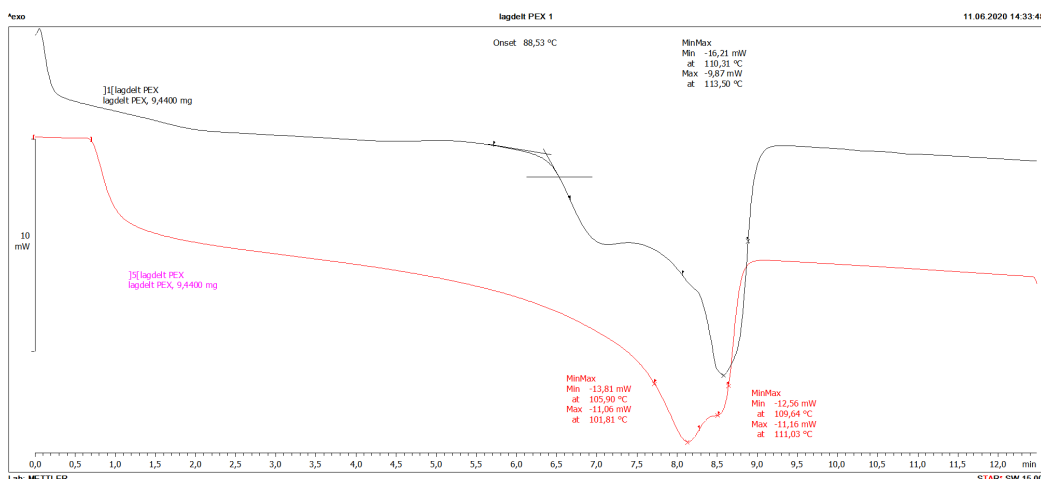

Figure A.1: DSC curve of layered sample.

---

[9]The samples used for DSC measurements were cut out from the same layered sample
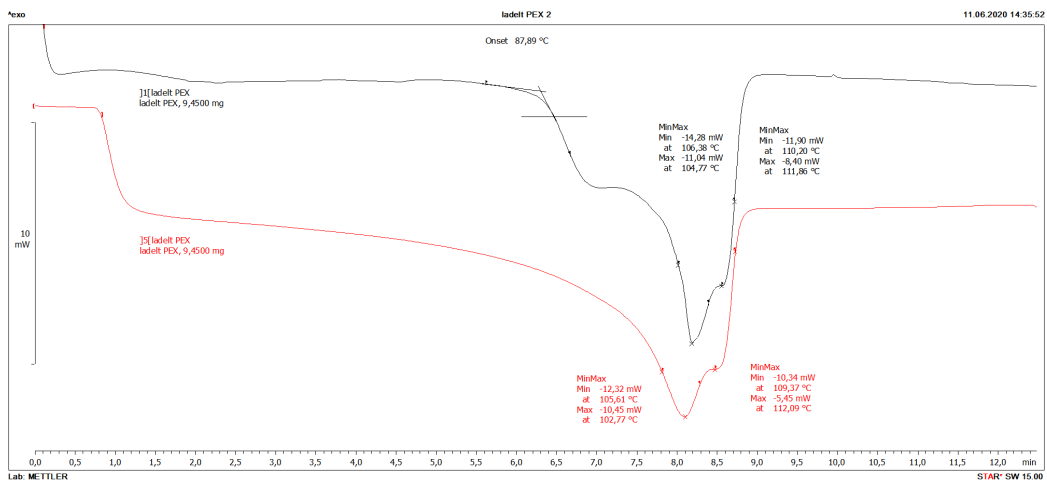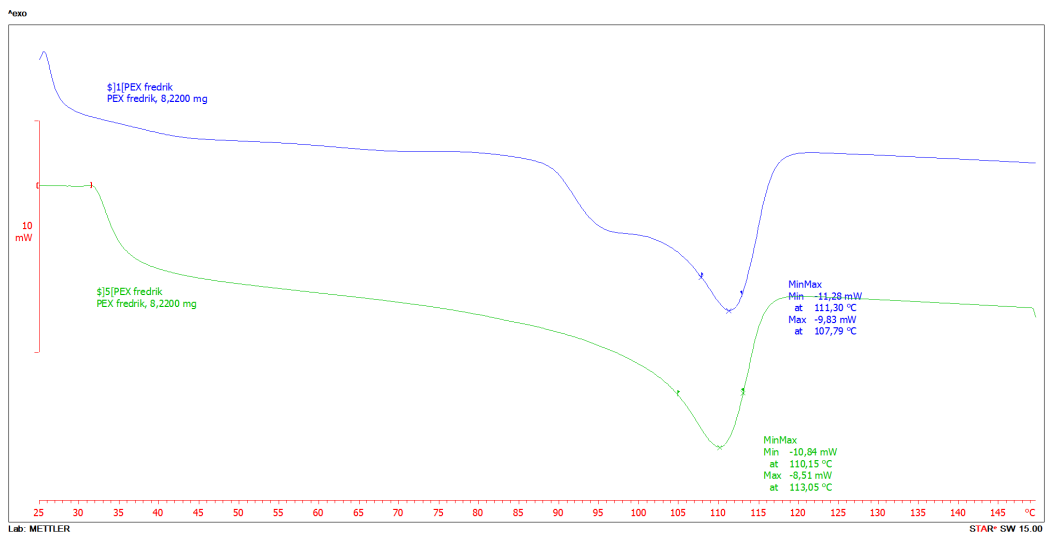
45

Figure A.2: DSC curve of layered sample. (2)

Figure A.3: DSC curve of XLPE sample.

46